32ND INTERNATIONAL COSMIC RAY CONFERENCE, BEIJING 2011

An Online Charge Calibration Method for LHAASO-WCDA Experiment

HANRONG WU[1], ZHIGUO YAO[1] FOR THE LHAASO COLLABORATION
[1]*Institute of High Energy Physics, BeiJing, 100049, China*
wuhr@mail.ihep.ac.cn

DOI: 10.7529/ICRC2011/V09/1123

Abstract: The prototype detector of LHAASO-WCDA experiment has found a two-peak structure in the distribution of PMT signals, yielded by near vertical cosmic muons in the water. A full Monte Carlo simulation, showing a very consistent result, verified that a proper measurement has been made. With the help of simulations, the mechanism for the origin of the second peak, produced by muons hit directly on the PMT, is well understood now. As a by-product, a method for the online charge calibration, making use of the second peak of muon signals, is proposed for the future WCDA experiment. Simulations indicate that this way of calibration can provide a precision of a few percents on the charge measurement. A dedicated calibration system based on this method has been implemented on the engineering array of WCDA, and its experimental performance is expected to be given soon.

Keywords: LHAASO, WCDA, charge calibration, cosmic muon, second peak, MC simulation.

1 Introduction

In prototype detector of LHAASO-WCDA experiment, A two-peak structure in the distribution of PMT signals has been found[1], and a full Monte Carlo simulation, showing a very consistent result. The first peak with low value is made up of pure geometrical effects of selected muons, and the second peak with high value is produced by muons directly hitting on the PMT photo-cathode. The second peak position represents the overall effects of PMT gain, quantum efficiency, photo-electron collecting efficiency, and front-end electronics without mixing the effect of water quality, so this provides a possible way for the WCDA to fulfill online charge calibration.

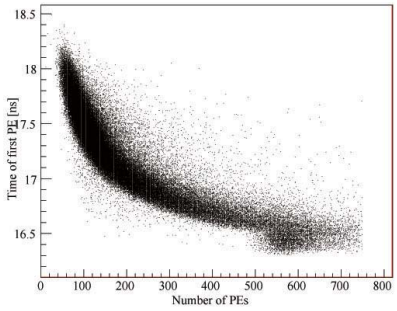

Figure 1: Time distribution of first photoelectron arriving at photocathode of PMT with the number of $N_{\rm pe}$.

2 The second peak

With the help of simulations, the mechanism for the origin of the second peak is welly understood. In the following part, it is described in two aspects: characteristics of distribution and production mechanism.

2.1 Characteristics of distribution of the second peak

In simulation, time distribution of first photoelectron arriving at the surface of photo-cathode of PMT as a function of $N_{\rm pe}$ is shown in figure 1. There is a bulge in the region of $N_{\rm pe}$ between the number of 500 and 600, which is consistent with the distribution of the number of photoelectrons (figure 2). In the configuration of simulation, the incident position of muons is on the plane of the top scintillator with z position of 274.5 cm, and z position of the top point of photo-cathode surface is about 488.5 cm, so the distance between the incident point and the surface of photocathode of PMT is about 488.3 cm, and transport time is $\sim$ 16.3 ns of the vertical muon arriving at the top surface of photocathode. Considering the fact that multi-scattering of muon and incident direction of are not totally vertical, transport time will be a little more longer than that. From this result, the second peak is made up of Cherenkov light emitted from muon hitting directly on the photocathode of PMT.

From the manufacture, photocathode ring radius of Hamamatu R5912 is about 10 cm. Figure 3 shows $N_{\rm pe}$ distribution of vertical muon signals detected by the PMT with gaussian fit for the second peak. Black line means $N_{\rm pe}$ distribution of vertical muon signals detected by the PMT (fit

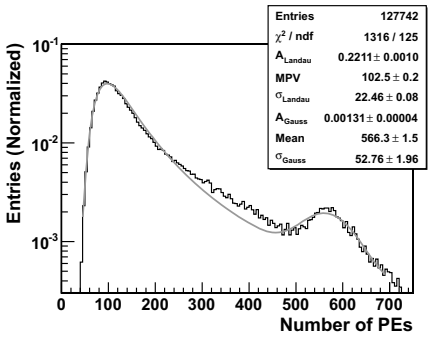

Figure 2: $N_{\rm pe}$ distribution of vertical muon signals detected by the PMT, superimposed with a Landau plus Gaussian fit for simulation results. The attenuation length of water, measured the same day data are taken, is 3.0 m.

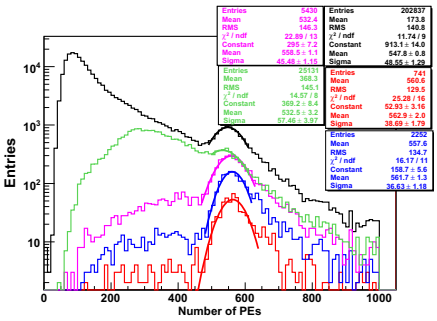

Figure 3: black line means $N_{\rm pe}$ distribution of vertical muon signals detected by the PMT; red line means distribution of muon hitting on the photocathode ring radius from 0 cm to 3 cm; blue line means distribution of muon hitting on the photocathode ring radius from 3 cm to 6 cm; pink line means distribution of muon hitting on the photocathode ring radius from 6 cm to 10 cm; green line means distribution of muon hitting on ring radius from 10 cm to 20 cm;

peak mean value 547.8); Red line means $N_{\rm pe}$ distribution of muon hitting on the photocathode ring radius from 0 cm to 3 cm (fit peak mean value 562.9); Blue line means $N_{\rm pe}$ distribution of muon hitting on the photocathode ring radius from 3 cm to 6 cm (fit peak mean value 557.6); Pink line means $N_{\rm pe}$ distribution of muon hitting on the photocathode ring radius from 6 cm to 10 cm (fit peak mean value 558.5); Green line means $N_{\rm pe}$ distribution of muon hitting on ring radius from 10 cm to 20 cm (fit peak mean value 532.5). This distribution shows that the position of the second peak has almost no relationship with hitting position of muon on photocathode of PMT.

2.2 Production mechanism of the second peak

As the paper[1] shows, the second peak is made up of most collected Cherenkov light emitted along a short track very near the PMT photo-cathode, which is about 6.3 cm, starting from about $H = 6.3$ cm above the PMT and ending at the PMT photo-cathode, and approximately 60 photo-electrons per cm track length can be collected by a PMT with a typical R5912 quantum efficiency, assuming a 100% geometrical efficiency and a 100% photo-electron collection efficiency. However, the position of the second peak gives a value of 89.9 photo-electrons per cm which is larger than 60, obtained from 566.3 (figure 2), and divide by 6.3 cm.

The spectrum of Cerenkov photons produced by a unit charge particle crossing a medium is given by the formula:

$$N_\gamma = \int\int 2\pi\alpha \sin^2\theta_{\rm c} \frac{1}{\lambda^2} \mathbf{d}_\lambda \mathbf{d}_x \propto \sin^2\theta_{\rm c} nx \qquad (1)$$

Where α is the fine structure constant and $2\pi\alpha = 0.04586$, $\sin^2\theta_{\rm c} = (1 - \frac{1}{\beta^2 n^2})$, where n is the medium index, for a relativistic particle $\beta = 1$, λ is the wavelength of the emitted light. Before arriving at the photo-cathode, the photon crosses two medium: water and glass. For water $n_{\rm water} = 1.33$ and $\theta_{\rm c} = 41.2°$, for glass $n_{\rm glass} = 1.5$ and $\theta_{\rm c} = 48.1°$, so in the medium glass, approximately 86 photo-electrons per cm track length can be collected. In simulation, the glass thickness of PMT is 3 mm, so in glass 25 more photo-electrons will be produced than in water with the same thickness.

There are some other possible factors: δ-ray production, muon multi-scattering, non-uniformity of photo-cathode, Rayleigh Scattering and Mie Scattering of photon, boundary effect between water and glass or glass and photo-cathode, which have effects on the distribution of photo-electrons. Through detailed simulation, the analysis results (figure 4) indicate that δ-ray production, non-uniformity of photo-cathode, boundary effect and the glass thickness of PMT contribute another more extra photo-electrons.

In figure 4, black solid line means $N_{\rm pe}$ distribution with a Gaussian fit for the second peak (peak mean value 564.2) including all process in simulation, red line means $N_{\rm pe}$ distribution (peak mean value 505.4) without the process δ-ray production and muon multi-scattering, blue one means $N_{\rm pe}$ distribution (peak mean value 487.7) with a uniform photo-cathode, pink one means $N_{\rm pe}$ distribution (peak mean value 439.2) without the process δ-ray production and muon multi-scattering and with a uniform photo-cathode, green one means $N_{\rm pe}$ distribution (peak mean value 391.3) without the process δ-ray production and muon multi-scattering and with a uniform photo-cathode and no boundary effect and with glass thickness about 0.01 mm. Therefore, δ-ray production and muon multi-scattering accounts for a percentage about $(487.7 - 439.2)/487.7 = 10\%$, non-uniformity of photo-cathode make a contribution about $(505.4 - 439.2)/505.4 = 13\%$, boundary effect and glass thickness of PMT makes a contribution about $(439.2 - 391.3)/439.2 = 11\%$. The latter two situation are related mutually. Considering quantum efficiency and track length, the difference of simulation and expectation value is about $391.3/6.3/60 = 4\%$. They are consistent very well.

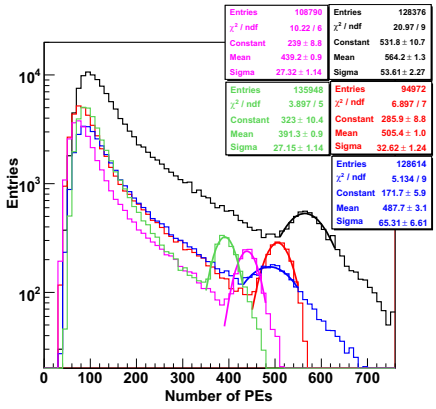

Figure 4: black solid line means $N_{\rm pe}$ distribution with a Gaussian fit for the second peak including all process in simulation, red line means $N_{\rm pe}$ distribution without the process δ-ray production and muon multi-scattering, blue one means $N_{\rm pe}$ distribution with a uniform photo-cathode, pink one means $N_{\rm pe}$ distribution without the process δ-ray production and muon multi-scattering and with a uniform photo-cathode, green one means $N_{\rm pe}$ distribution without the process δ-ray production and muon multi-scattering and with a uniform photo-cathode and no boundary effect and with glass thickness about 0.01 mm.

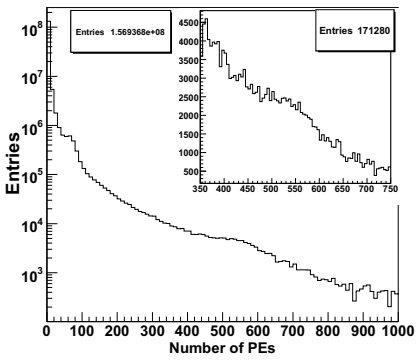

Figure 5: $N_{\rm pe}$ distribution of muon and background on PMT.

3 Charge calibration

As mentioned above, the second peak position can provide an effective way for the WCDA to online calibration and monitor the PMT and electronics in the measurement of charge. In the following part, with the help of simulation, the calibration method is discussed; and an introduction to engineering project is given.

3.1 Calibration method

In figure 2, the second peak is observed using three fold coincidence of scintillator to select events. If there is no scintillator to make event selection, distribution of number of $N_{\rm pe}$ of muon and background detected by PMT is shown in figure 5, and a local plot at the second peak is shown in the same canvas, which is too flat to be fitted at position of the second peak. Statistics of this sample is estimated to be $\sim$ 4 hours for online data taking, and if we make charge calibration every 10 days, there will be $\sim 1.7\%$ dead time, which is large, so this method is not effective. An effective way we bring up is that a shading pad is put above PMT to lower down background.

Firstly, with the help of simulation, performance of online calibration is studied. A parameterized function for muon direction and momentum, with flux adjusted by the vertical muon spectrum from the CAPRICE measurement (extrapolated to sea level), is used to sample the muon event. In simulation, muon events from all directions and energy range are selected, and in order to save CPU time, the events which can arrive at the bottom of the water tank are simulated. In order to screen most cherenkov light produced by electromagnetic particle, a curtain with some distance from the top of PMT photo-cathode is set up. Area of the curtain is $1\ {\rm m} \times 1\ {\rm m}$, and thickness is 1 mm.

In simulation, the curtain heights from the top surface of PMT: 10 cm, 13 cm, 14 cm, 14.5 cm, 15 cm, 16 cm, 16.5 cm, 17 cm, 30 cm, 40 cm are tried to find a appropriate value. The result is shown in figure 6. The top picture is a function of the second peak mean value by Gaussian fit with the curtain heights, the bottom picture is a variation percentage between two neighbouring variable height. The results indicate that uncertainty of the curtain position from 14 cm to 40 cm only have about 2% difference.

Considering the feasibility of online calibration, online data taking time with the statistics satisfied with a good precision is estimated to be ~ 1.48 hours, and the curtain height is selected 15 cm from top surface of PMT photo-cathode. The results is shown in figure 7, with a good fit precision. Contribution of electromagnetic secondary particle to the second peak is simulated, the result is shown in figure 8; and total Contribution of muon plus electromagnetic secondary particle to the second peak is shown in figure 9, and event rate is about 176 Hz, which is very low and can be supported by WCDA electronics. The results also indicate that the electromagnetic secondary particle has almost no effect (fit peak value 520.5 from figure 7 and 518.3 from figure 9) on the second peak position after adding a curtain.

3.2 Engineering project

A dedicated calibration system based on this method has been implemented on the engineering array of WCDA. There are two girders with a distance of 50 cm from the bottom, and between the two girders there is a shielding plate, which can slide along the girders pulled by Polyamide fixed on two ends of the plate using staples. when the shading pad moves to the fixed screws on one end of the girders, PMT is at the bottom center of it with a distance of about

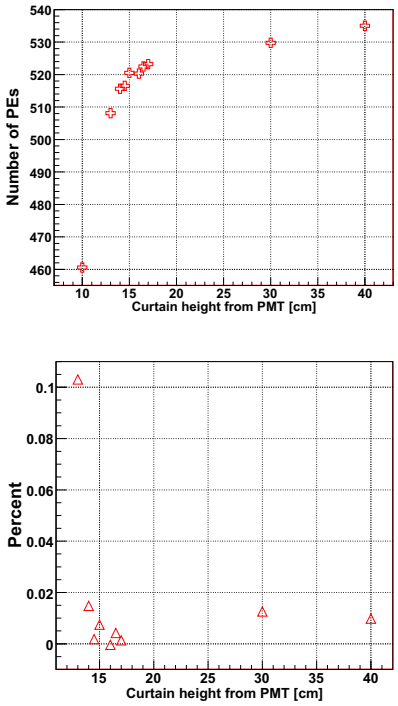

Figure 6: The top picture is a function of the second peak mean value by Gaussian fit with the curtain heights, the bottom picture is a variation percentage between two neighbouring variable height.

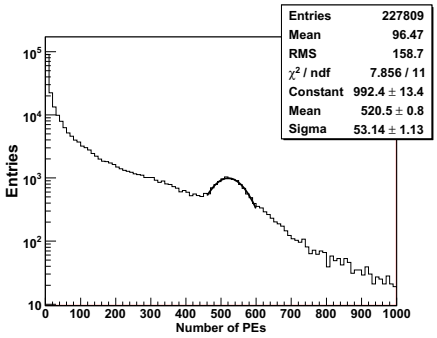

Figure 7: N_{pe} distribution of muon signals detected by the PMT, a curtain ($1\ \mathrm{m} \times 1\ \mathrm{m} \times 1\ \mathrm{mm}$) is set up with the distance 15 cm from top of PMT photo-cathode.

15 cm from the top surface of PMT (figure 10). When the shading pad moves to another end of the girders, there is nothing on the top of PMT. Its experimental performance is expected to be given soon.

4 Conclusion

After detailed simulation study, the origin of the second peak is well understood, and simulation result indicates that the way of online charge calibration is effective.

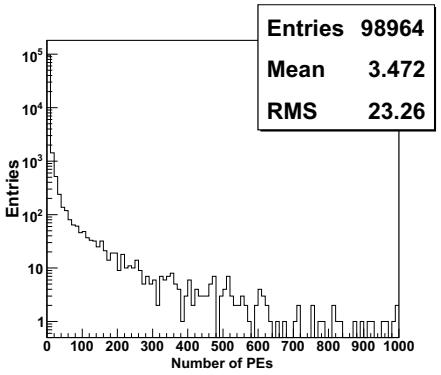

Figure 8: N_{pe} distribution of electromagnetic secondary particle detected by the PMT, a curtain ($1\ \mathrm{m} \times 1\ \mathrm{m} \times 1\ \mathrm{mm}$) is set up with the distance 15 cm from top of PMT photo-cathode.

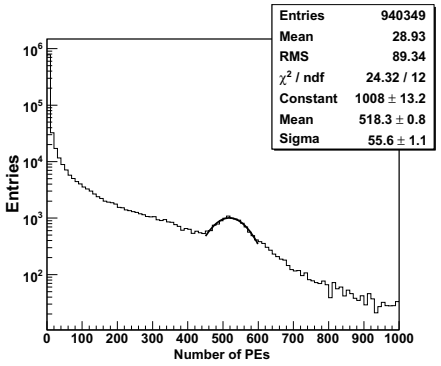

Figure 9: N_{pe} distribution of muon signals and electromagnetic secondary particle detected by the PMT, a curtain ($1\ \mathrm{m} \times 1\ \mathrm{m} \times 1\ \mathrm{mm}$) is set up with the distance 15 cm from top of PMT photo-cathode.

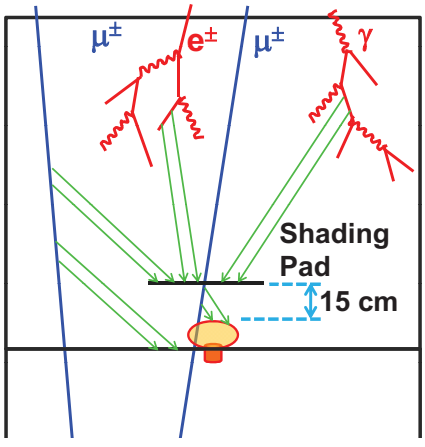

Figure 10: sketch map of charge calibration

References

[1] Q. An, et al., Nucl. Instr. and Meth. A (2011), doi:10.1016/j.nima.2011.04016